Electronic supplementary Information (ESI)

Carbon Nanotubes to Outperform Metal Electrodes in Perovskite Solar Cells via Dopant Engineering and Hole-Selectivity Enhancement

Il Jeon,[*‡ab] Ahmed Shawky,[‡ac] Seungju Seo,[a] Yang Qian,[a] Anton Anisimov,[d] Esko I. Kauppinen,[e] Yutaka Matsuo,[*a,f] Shigeo Maruyama[*a,g]

[a]*Department of Mechanical Engineering, The University of Tokyo 7-3-1 Hongo, Bunkyo-ku, Tokyo 113-8656, Japan*

[b]*Department of Chemistry Education, Graduate School of Chemical Materials, Institute for Plastic Information and Energy Materials, Pusan National University, 63-2 Busandaehak-ro, Busan 46241, South Korea*

[c]*Nanomaterials and Nanotechnology Department, Advanced Materials Division, Central Metallurgical R&D Institute (CMRDI), P.O. Box 87 Helwan, Cairo 11421, Egypt*

[d]*Canatu, Ltd., Konalankuja 5, FI-00390 Helsinki, Finland*

[e]*Department of Applied Physics, Aalto University School of Science, P.O. Box 15100, FI-00076 Aalto, Espoo, Finland*

[f]*Institute of Materials Innovation, Institutes of Innovation for Future Society, Nagoya University, Furo-cho, Chikusa-ku, Nagoya 464-8603, Japan*

[g]*Energy NanoEngineering Lab., National Institute of Advanced Industrial Science and Technology (AIST), Tsukuba, 305-8564, Japan*

AUTHOR INFORMATION

***Corresponding Authors**

*il.jeon@spc.oxon.org; *matsuo@photon.t.u-tokyo.ac.jp; *maruyama@photon.t.u-tokyo.ac.jp

Experimental Methods

Aerosol CNT films Preparation. CNTs were synthesised by an aerosol (floating catalyst) CVD method based on ferrocene vapour decomposition in a CO atmosphere. The catalyst precursor was vaporised by passing ambient temperature CO through a cartridge filled with ferrocene powder. The flow containing ferrocene vapour was then introduced into the high-temperature zone of a ceramic tube reactor through a water-cooled probe and mixed with additional CO. To obtain a stable growth of CNTs, a controlled amount of CO_2 was added together with the carbon source, CO. CNTs were directly collected downstream of the reactor by filtering the flow through a nitrocellulose membrane filter (Millipore Corp., USA; HAWP, 0.45 μm pore diameter). The time of collection determines the transparency and the conductivity of the CNT films.

$MAPbI_3$ solution preparation. CH_3NH_3I (Aldrich), PbI_2 (TCI), and anhydrous dimethyl sulfoxide (TCI) (molar ratio 1:1:1) were mixed in anhydrous *N,N*-dimethylformamide (TCI) with a concentration of 50 wt%. The solution was filtered through a 0.2 μm poly(tetrafluoroethylene) filter before use.

Perovskite Solar Cell Fabrication. ITO patterned glass substrates were cleaned and sonicated with detergent, distilled water, acetone, and isopropanol in an ultrasonic bath for 15 min, respectively. The cleaned substrates underwent the UV-ozone for wettability enhancement and removal of any organic contamination. 30 millimolar $SnCl_2 \cdot 2H_2O$ (Aldrich, >99.995%) solution in ethanol (anhydrous, Fujifilm Wako Pure Chemical Co.) as a precursor solution was used for deposition of a compact SnO_2 layer. The solution was filtered by a 0.2 μm syringe filter, followed by spin-coating on the cleaned substrate at 3000 rpm for 30 s. The spin-coated film was annealed at 165 °C for 30 min. After cooling down to room temperature, another cycle of the spin-coating

process was repeated, which was followed by annealing at 150 °C for 5 min and 190 °C for 1 h. The SnO_2-coated ITO glass was treated with UV-ozone before spin-coating of the prepared perovskite solution. Then, 20 μL of perovskite precursor solution was spin-coated onto the SnO_2 layer at 4000 rpm for 20 s, with 0.15–0.30 mL of anhydrous diethyl ether slowly dripped onto the substrate 12 s after the start of the spin-coating process. Next, the film was annealed at 100 °C for 10 min to obtain a dense brown $MAPbI_3$ film.

For the CNT-based devices, pre-cut CNT films of different transparencies (active area 5x2 mm^2) were laminated on the top of the prepared $MAPbI_3/SnO_2$/ITO/glass substrates to room temperature by applying press-transfer method on the perovskite surface just after cooling. Before depositing the hole transporting layer (HTL), a 20 μL solution containing different concentrations of TFMS in ODCB (0.01, 0.015, 0.02, 0.025 and 0.05 wt%) was spin-coated on the CNT-laminated PSCs at 300 rpm for 30 s. Then, the HTL solution was prepared by dissolving 85.8 mg of spiro-MeOTAD (Merck) in 1 mL of chlorobenzene (anhydrous, 99.8%, Sigma-Aldrich) which was mixed with 33.8 μL of 4-tert-butylpyridine (96%, Aldrich) and 19.3 μL of Li-TFSI (99.95%, Aldrich, 520 mg mL^{-1} in acetonitrile) solution. Different concentrations of HTL tested were by a factor of 0.9, 0.95, 1.0, 1.05, 1.085, 1.17, 1.25, and 1.4. The spiro-MeOTAD solution was spin-coated on the perovskite layer at 3000 rpm for 30 s by dropping 20 μL of the solution. The fabrication was finally completed by thermal evaporation of a 50-nm-thick film of gold electrode (3x3 mm^2 active area) for the reference devices only at a constant evaporation rate of 0.05 nm s^{-1}.

Characterisations. The $J-V$ curves were measured using a software-controlled source meter (Keithley 2400 Source-Meter) under dark conditions and the simulated sunlight irradiation of 1 sun (AM 1.5G; 100 mW cm^{-2}) using a solar simulator (EMS- 35AAA, Ushio Spax Inc.) with a Ushio Xe short arc lamp 500. The source meter was calibrated using a silicon diode (BS-520BK,

Bunkokeiki). By using Agilent 4156C analyser with a four-probe station, the sheet resistance of CNT films were measured (van der Pauw method). The SEM analysis of the CNTs and device cross-section were performed using an S-4800 (Hitachi) electron microscope. The SEM images were analysed by ImageJ software. An inVia Raman microscope (Renishaw) was employed for the vibrational spectra observation of CNT and doped-CNT electrodes with 532 nm laser wavelength. Shimadzu UV-3150 was used for the UV−Vis−NIR measurement. The PL measurements were performed using JASCO Spectrofluorometer (FP-8300). The valence band and the Fermi levels measurements were performed using Riken Keiki PYS-A AC-2 and Kelvin probe spectroscopy in air (ESA), respectively. A source measurement unit was used to record the current at each specific wavelength. Solartron SI1287 Electrochemical Interface and Solartron 1255B Frequency Response Analyser were used for the Impedance Measurement.

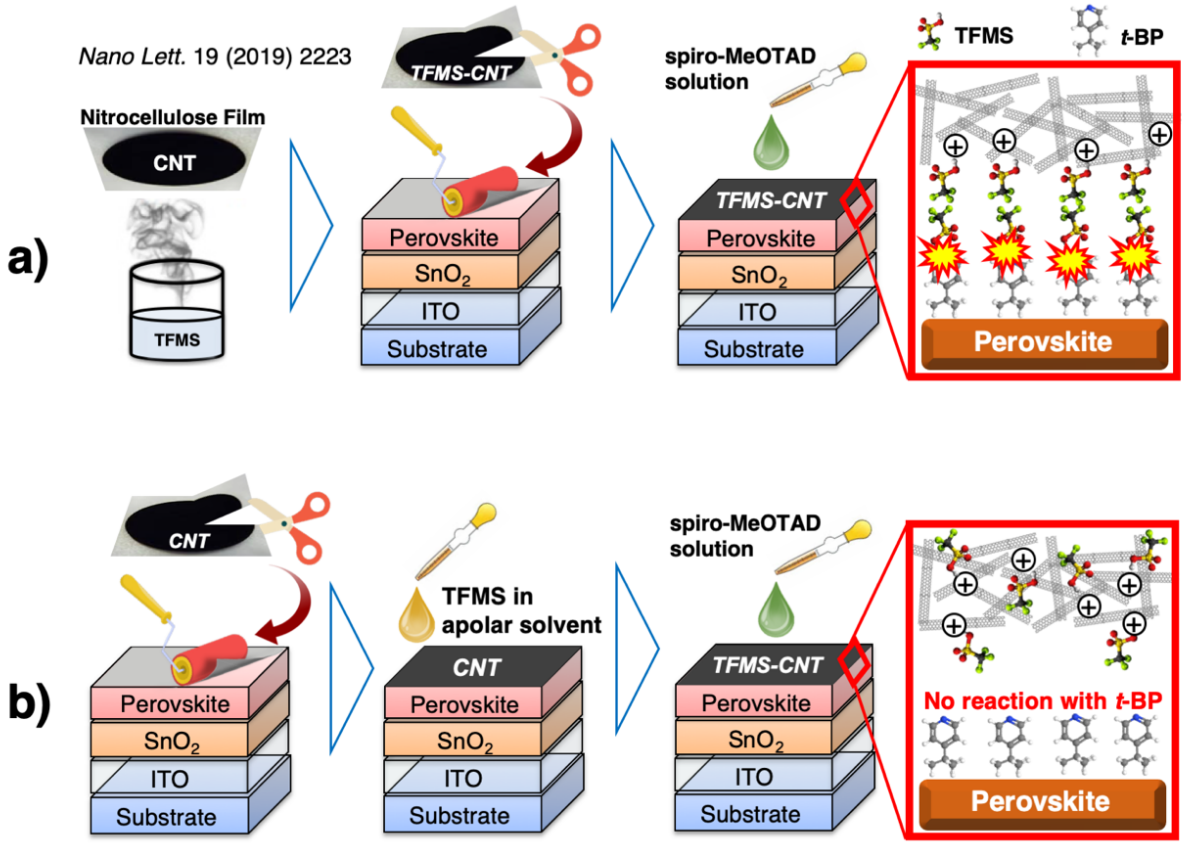

Fig. S1. Illustration of top CNT electrode *p*-doping and fabrications a) of our previous work (Reproduced with permission [17] Copyright 2017, American Chemical Society) and b) of this work.

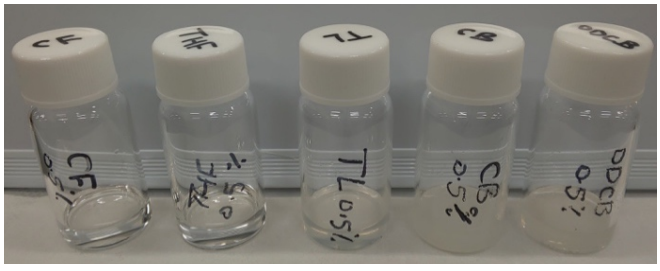

Fig. S2. TFMS dispersed in various non-polar solvent (CF, THF, toluene, CB and ODCB). The solution appears transparent or murky depending on solvents.

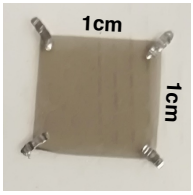

Fig. S3. Indium contact applied T60% CNT for the four probe Van der Pauw method.

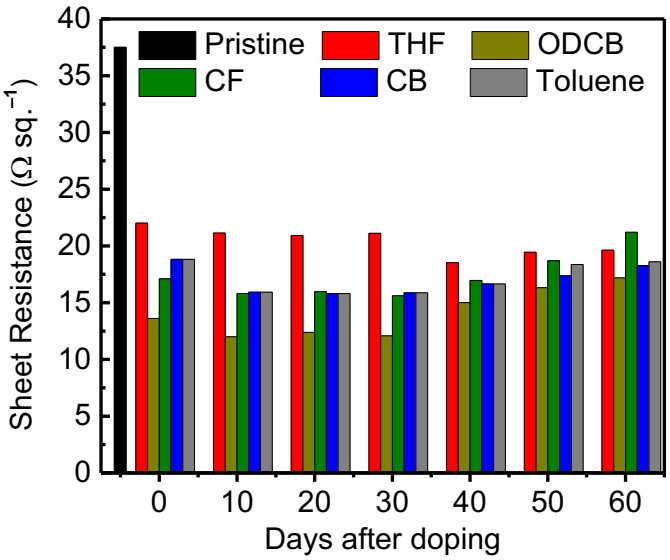

Fig. S4. A bar graph showing the sheet resistance changes upon TFMS doping in different apolar solvents and their durability.

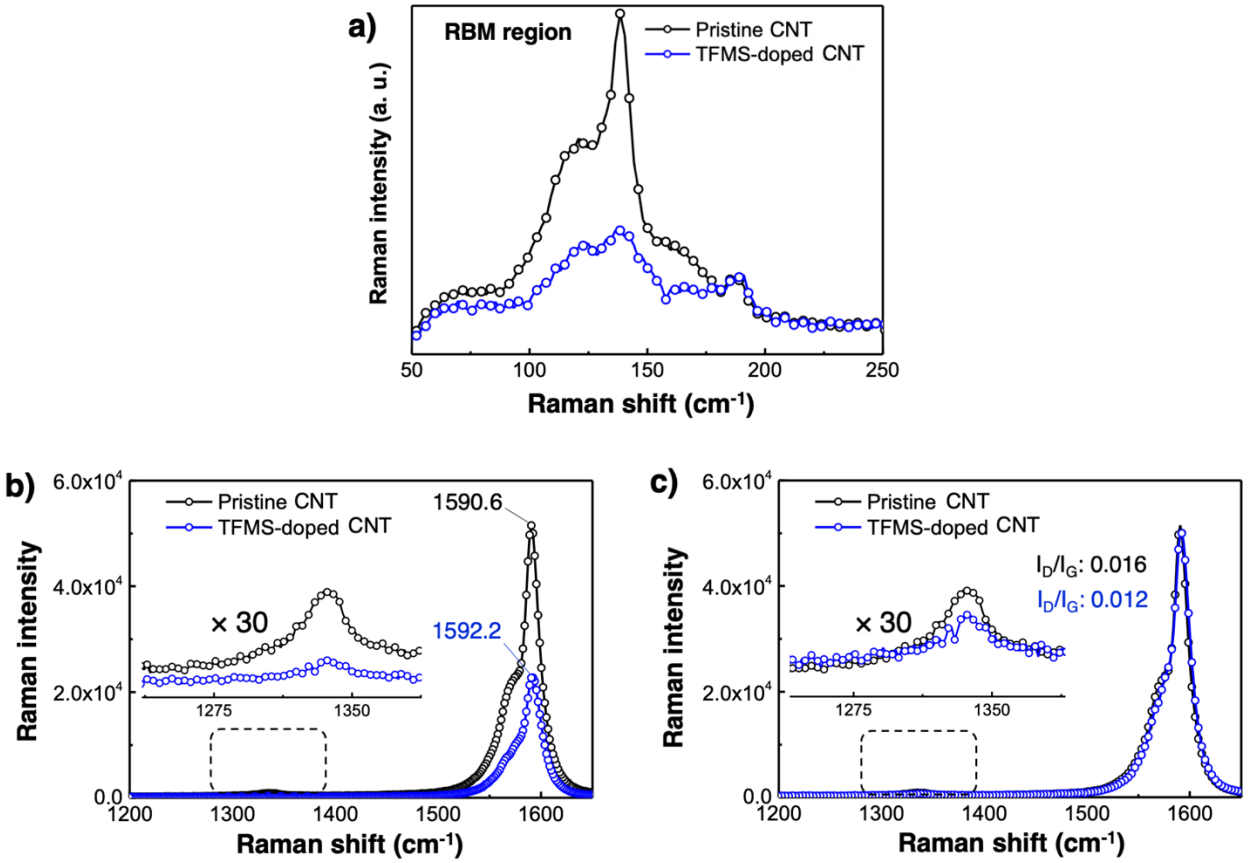

Fig. S5. a) RBM region, b) the G-band, and c) The G-to-D ratio of the Raman spectra of a pristine CNT film (black), and a TFMS-applied CNT film.

Table S1. Photovoltaic parameters of varying concentrations of TFMS-applied CNT-based PSCs under AM1.5G 1 sun illumination.

TFMS conc.	J_{SC} (mA cm^{-2})	V_{OC} (V)	FF	PCE (%) [average ±error]
0	19.8	0.97	0.59	11.3 [10.3 ±0.73]
0.010 wt.%	20.3	1.00	0.60	12.1 [10.8 ±0.90]
0.015 wt.%	20.6	1.03	0.62	13.2 [12.4 ±0.60)
0.020 wt.%	15.9	0.87	0.49	6.9 [6.5 ±0.35]
0.025 wt.%	15.5	0.80	0.40	5.0 [4.5 ±0.63]
0.050 wt.%	4.6	0.66	0.33	1.1 [0.84 ±0.28)

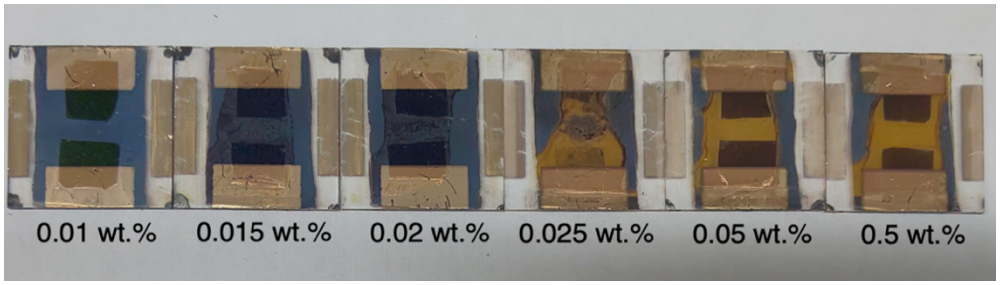

Fig. S6. Pictures of the CNT-PSCs upon various concentrations of TFMS application.

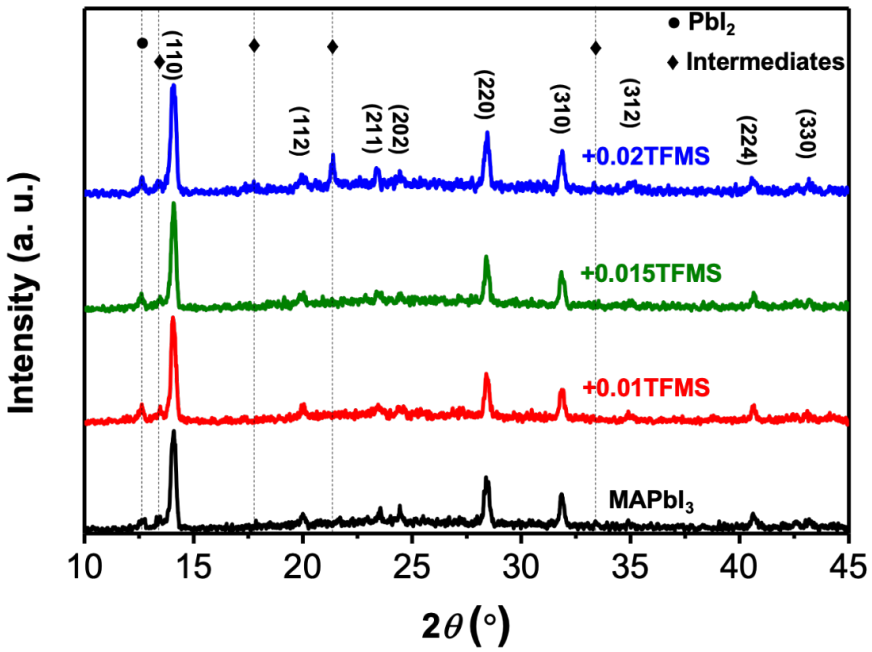

Fig. S7. XRD spectra of the perovskite films after various concentrations of TFMS doping.

Table S2. Photovoltaic parameters of CNT-PSCs upon TFMS doping and spiro-MeOTAD application under AM1.5G 1 sun illumination.

Device type	J_{SC} (mA cm^{-2})	V_{OC} (V)	FF	R_S (Ω)	R_{SH} (× 10^4 Ω)	PCE
Pristine	19.8	0.97	0.59	62.9 ±7.6	1.5 ±1.3	11.4%
TFMS-doped	20.6	1.03	0.62	51.5 ±2.4	2.3 ±2.1	13.2%
HTL-applied	21.7	1.04	0.67	57.7 ±9.8	5.6 ±2.7	15.3%
TFMS-doped & HTL-applied	1.08	1.08	0.69	51.5 ±4.7	10 ±3.0	17.0%

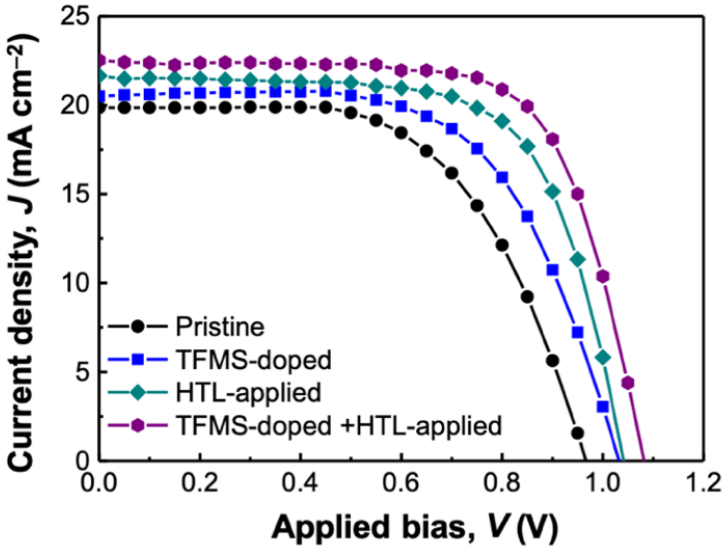

Fig. S8. *J–V* curves of the CNT-PSC (black circles), the 0.15 wt.% TFMS-doped CNT-PSC (blue squares), the HTL-applied CNT-PSC (turquoise diamonds), and the 0.15 wt.% TFMS-doped HTL-applied CNT-PSC (purple circles).

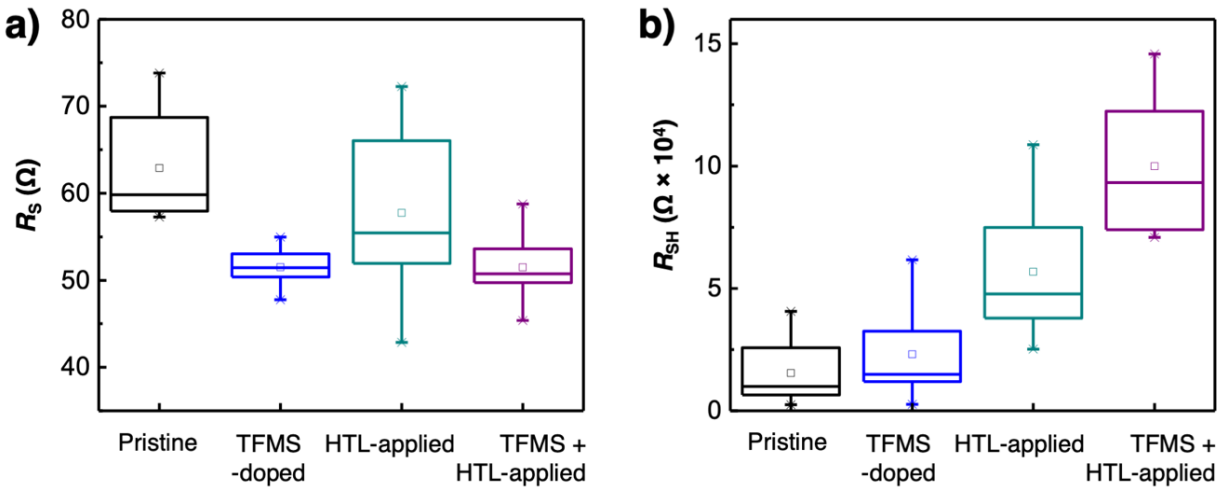

Fig. S9. a) R_S and b) R_{SH} values of the CNT-PSC (black), the TFMS-doped CNT-PSC (blue), the HTL-applied CNT-PSC (turquoise), and the TFMS-doped HTL-applied CNT-PSC (purple).

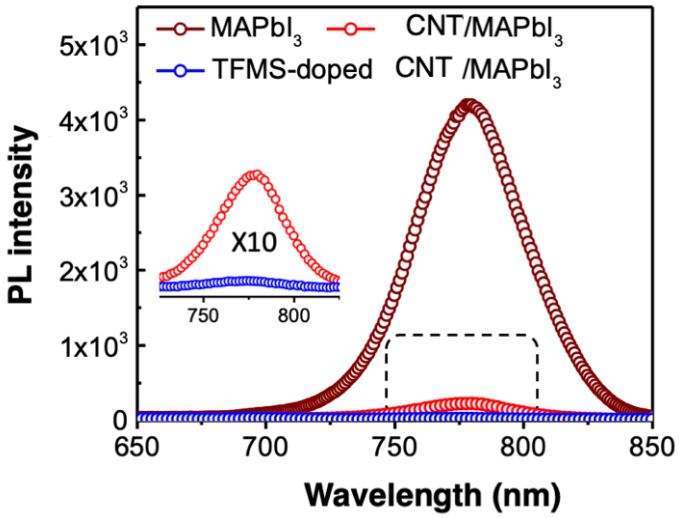

Fig. S10. PL spectra of the $MAPbI_3$ film (brown), CNT on the $MAPbI_3$ film (red), and TFMS-doped CNT on the $MAPbI_3$ film (blue).

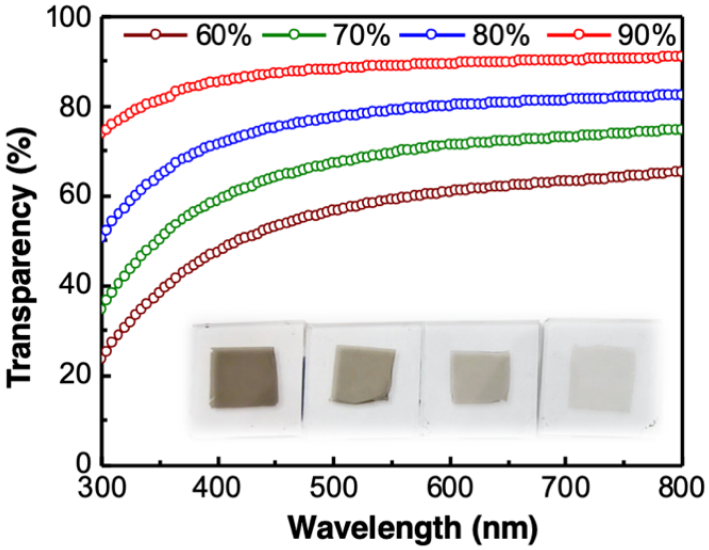

Fig. S11. Transmittance spectra of CNT films with different densities, namely, T90%-CNT (red squares), T80%-CNT (blue squares), T70%-CNT (green squares), and T60%-CNT (brown squares) and the photos as an inset.

Table S3. Sheet resistance of CNT films with different densities before and after doping.

CNT type	Sheet Resistance (Ω sq.$^{-1}$)	After 0.05 wt.%TFMS doping (Ω sq.$^{-1}$)
T90%	100 ±12.1	81 ±14.0
T80%	80.9 ±1.25	68.8 ±2.74
T70%	57.4 ±1.72	35.5 ±3.98
T60%	36.5 ±0.88	28.4 ±1.82

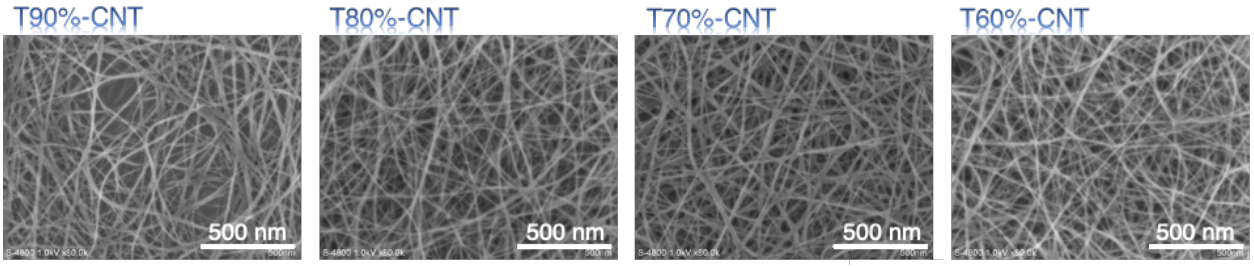

Fig. S12. SEM images of T90%-CNT, T80%-CNT, T70%-CNT and T60%-CNT.

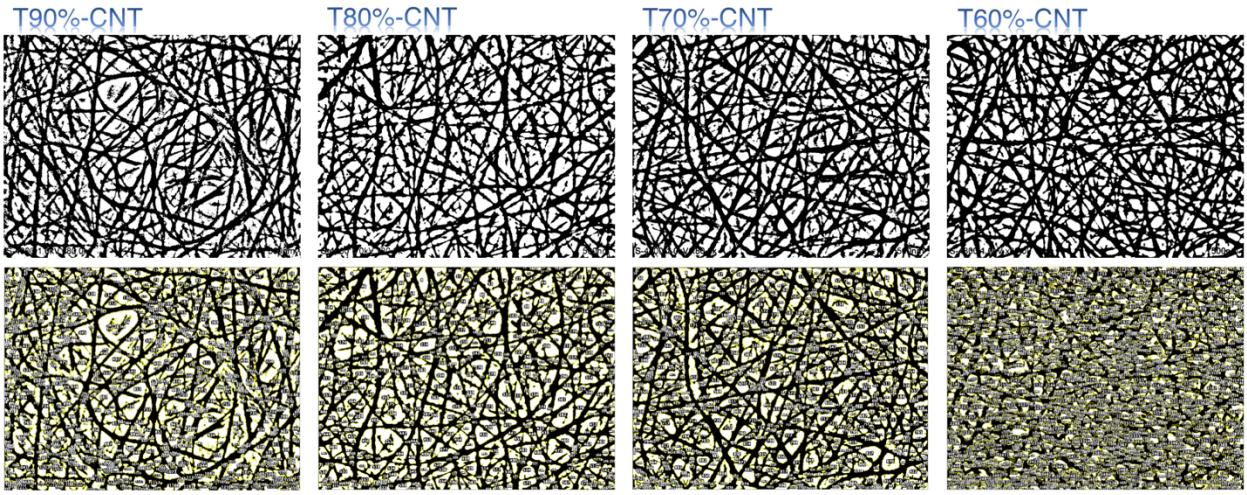

Fig. S13. Processed SEM images of T90%-CNT, T80%-CNT, T70%-CNT and T60%-CNT.

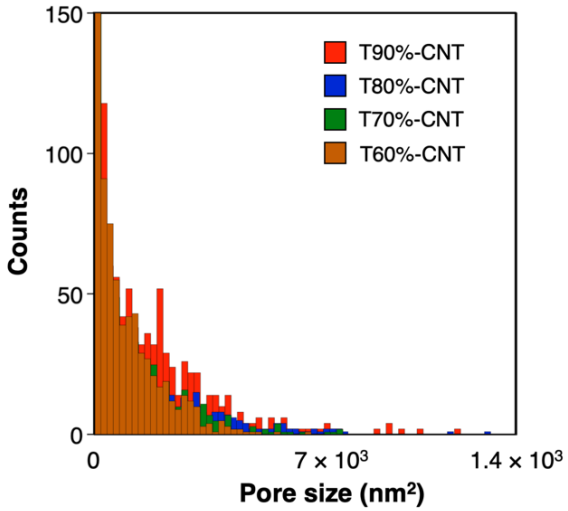

Fig. S14. Pore size distribution of different CNT density films as indicated.

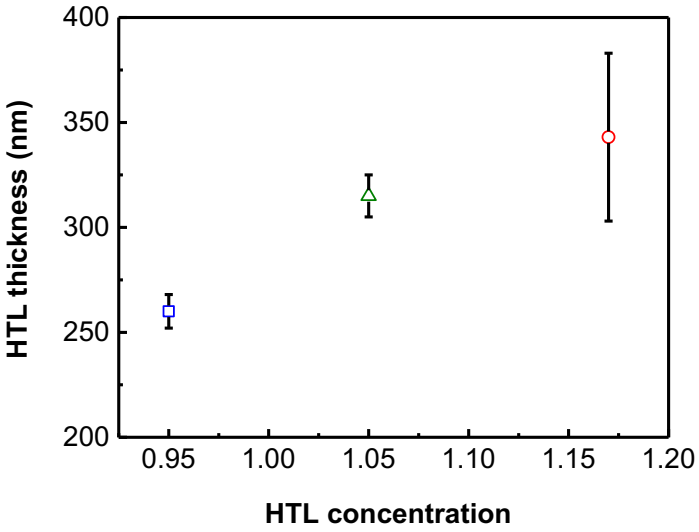

Fig. S15. Thickness of spiro-MeOTAD on a perovskite film measured by a profilometer.

Table S4. Thickness of spiro-MeOTAD on a perovskite film measured by a profilometer.

HTL concentration	Thickness(nm)
x 0.95	260±8
x 1.05	315±10
x 1.17	343±40

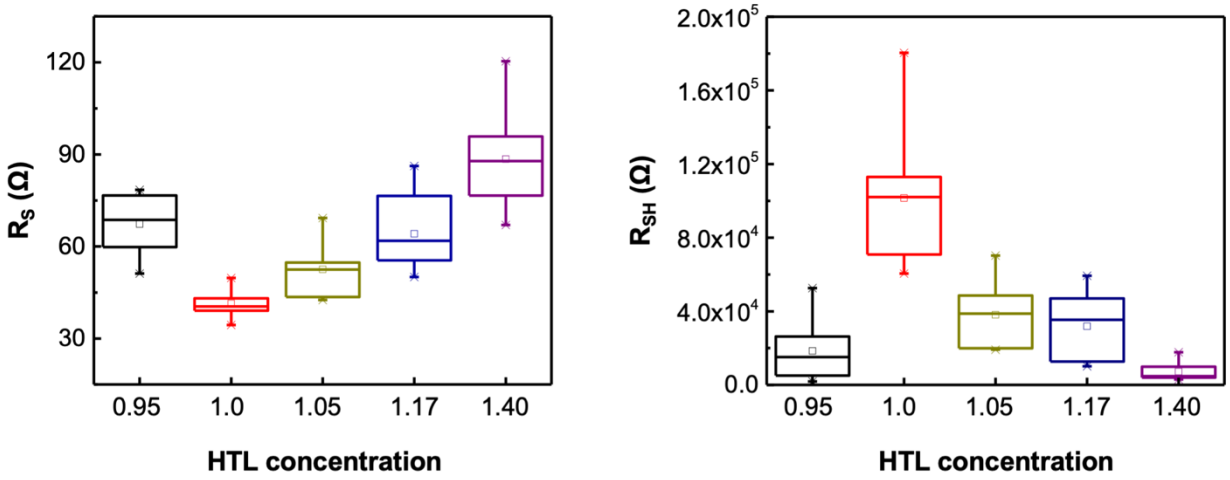

Fig. S16. R_S and R_{SH} of different spiro-MeOTAD concentrations in Au-based PSC devices.

Table S5. R_S and R_{SH} of different spiro-MeOTAD concentrations in Au-based PSC devices.

HTL concentration	R_S (Ω)	R_{SH} (x10^4 Ω)
x 0.95	67.3±10.1	1.8±1.7
x 1.00	41.1±4.4	10.1±3.7
x 1.05	52.5±8.8	3.8±1.9
x 1.17	64.1±12.8	3.2±1.8
x 1.40	88.5±16.8	0.7±0.5

Table S6. R_S and R_{CT} values derived from the Nyquist plot of the EIS measurement.

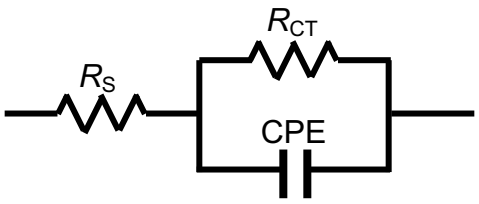

HTL conc.	R_S (Ω)	R_{CT} (Ω)
x0.95	32.5	106.2
x1.05	26.2	142.8
x1.17	23.5	157.1

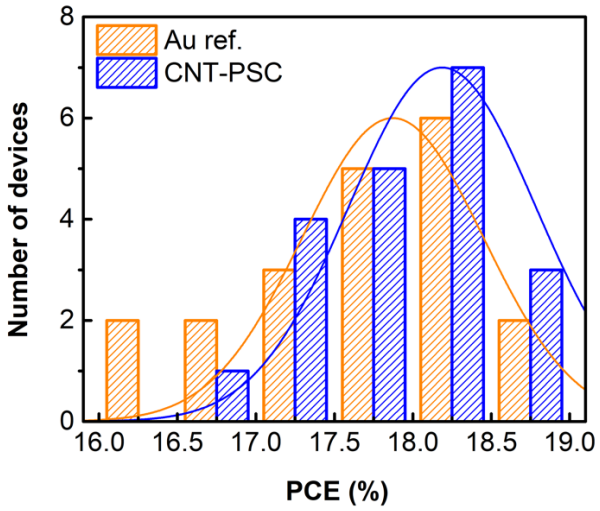

Fig. S17. Statistical analysis of PCEs of the Au-based PSCs and the CNT-based PSCs collected from 20 devices each.

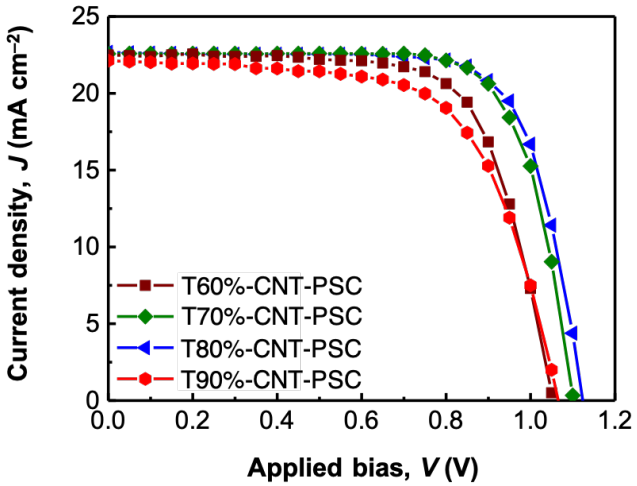

Fig. S18. *J–V* curves of the champion T60%-CNT-PSC (brown square), T70%-CNT-PSC (green diamond), T80%-CNT-PSC (blue triangle) and T90%-CNT-PSC (red hexagon).

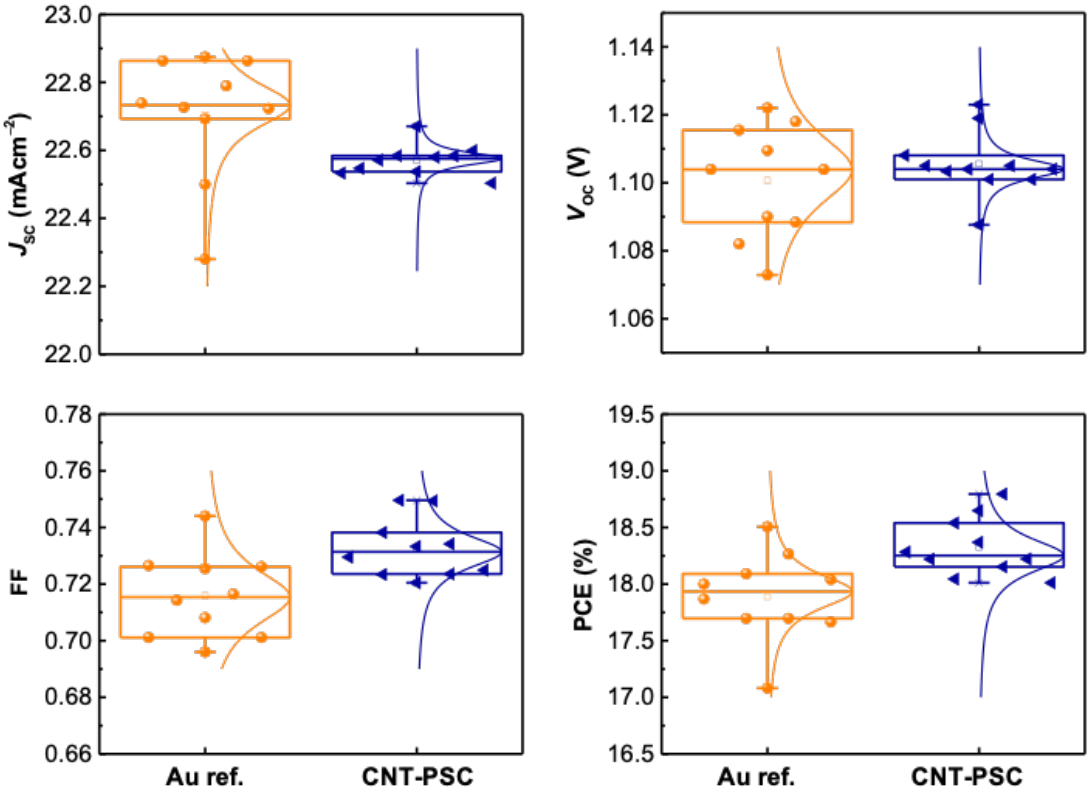

Fig. S19. Statistical analyses of the photovoltaic parameters from the best 10 devices with the device points (Fig. 5c).

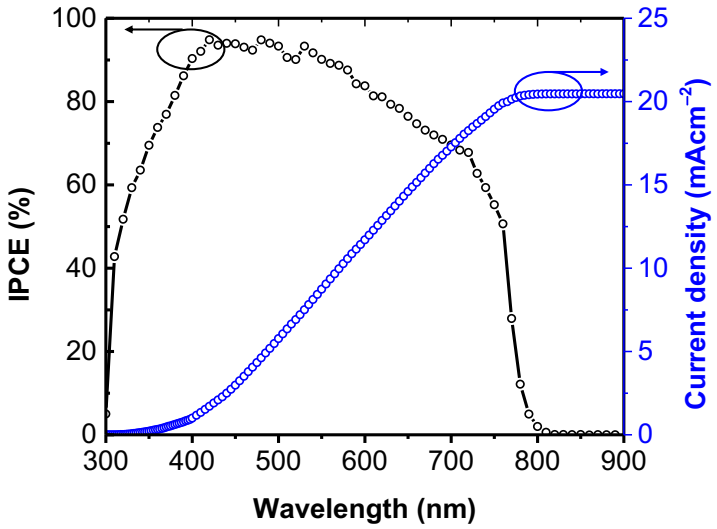

Fig. S20. IPCE (black line) and accumulative current density (red line) of the T80%-CNT-PSC.

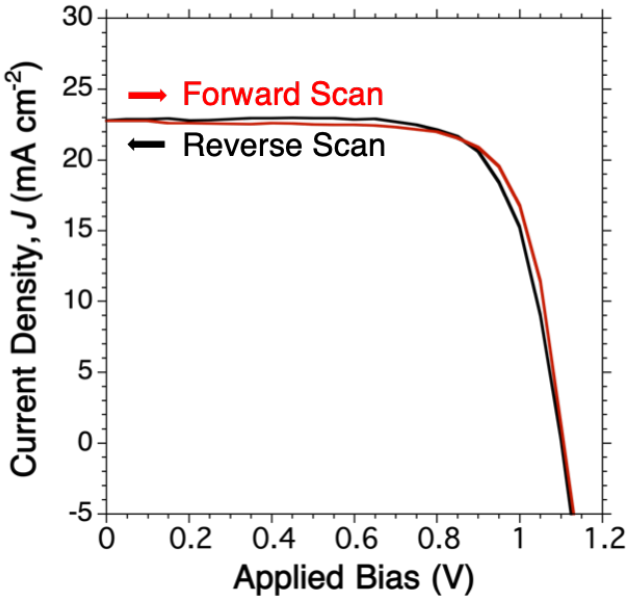

Fig. S21. *J–V* curves of the T80%-CNT-PSC with both scan directions.

Table S7. Reported PCEs of the CNT-based PSCs. SWNT stands for single-walled CNT, DWNT stands for double-walled CNT, CSCNT stands for cross-stacked CNT and MWNT stands for multi-walled CNT. The citation numbers are referenced to the reference list of the main text.

	Year	CNT Type	Electrode Type	PCE (%)	Control (%)	Citation
n/a	2020	SWNT	Top Electrode	18.8	18.4	This work
a	2019	DWNT	Bottom Electrode	17.2	n/a	[42]
b	2018	SWNT	Top Electrode	17.56	n/a	[17]
c	2018	SWNT	Top Electrode	15.3~17	n/a	[13]
d	2018	CSCNT(MWNT)	Top Electrode	11.9	n/a	[48]
e	2018	SWNT	Top Electrode	11.8	n/a	[47]
f	2017	SWNT	Top Electrode	16.6	18.4	[12]
g	2017	SWNT	Bottom Electrode	15.3	17.7	[29]
h	2017	B-doped MWNT	Top Electrode	14.6	n/a	[49]
i	2017	CSCNT (MWNT)	Top Electrode	14.3	16 (rigid)	[50]
j	2017	SWNT/NiO	Top Electrode	12.7	n/a	[51]
k	2016	SWNT	Top Electrode	15.5	18.8	[52]
l	2016	C/SWNT	Top Electrode	14.7	n/a	[53]
m	2016	CSCNT (MWNT)	Top Electrode	10.54	14.76	[54]
n	2015	MWNT	Top Electrode	12.67	n/a	[55]
o	2015	SWNT	Bottom Electrode	6.32	9.5	[56]
p	2015	Twisted MWNT fiber	Top Electrode	3.03	2.8	[57]

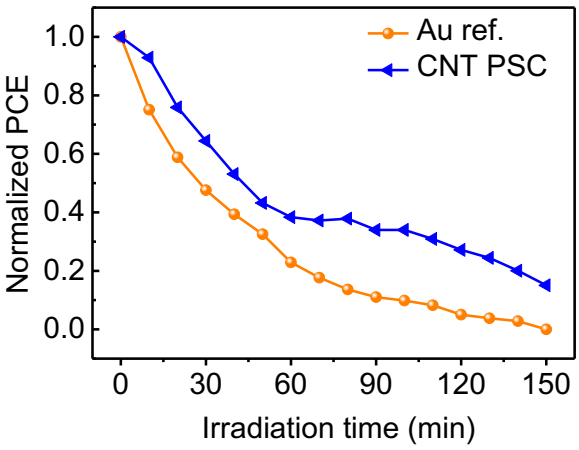

Fig. S22. Device stability data of the unencapsulated Au-based PSC (orange circles) and the unencapsulated TFMS-treated T80%-CNT-PSC (blue triangles) under constant illumination of one sun.